DIRECT DETECTION ANALOG NONLINEAR MIMO FOR MODE-DIVISION MULTIPLEXING IN FIBER

A. Spalvieri, P. Boffi, S. Pecorino, M. Magarini, A. Gatto, P. Martelli, M. Martinelli
Dipartimento di Elettronica, Informazione e Bioingegneria, Politecnico di Milano, Italy
L. Barletta
Institute for Advanced Study, Technische Universität München, Germany

Complexity of digital multiple-input multiple-output (MIMO) signal processing based on coherent detection affects the development of mode division multiplexing systems. The inherent characteristics of fiber modes is here exploited to get a nonlinear MIMO system based on direct detection by circular photodiodes and analog non-adaptive electrical network.

1. Introduction

MODE Division Multiplexing (MDM) is an additional dimension with respect to the wavelength [1] and the polarization [2] to increase the capacity over a single fiber, in order to keep up with the demands in data traffic growth, both in long-haul transmission, in access networks and in data server interconnections. Critical issues when MDM transmission is performed are the mode demultiplexing before the receiver and the mode crosstalk induced during the fiber propagation. In recent experiments, MDM is successfully applied by exploiting multiple-input multiple-output (MIMO) digital signal processing (DSP) in combination with coherent detection [3], [4]. This technique, generally applied to linearly-polarized (LP) modes, allows to process each mode, increasing capacity. Real-time MIMO processing requires high-speed DSP. In order to achieve mode demultiplexing and to counteract mode crosstalk, the hardware cost increases linerly with number of modes and the complexity of the DSP is proportionally to the square of number of modes [5]. System solutions operating with low MIMO-DSP complexity have been proposed [6], performing optical demultiplexing before coherent detection. Nowadays, optical mode demultiplexing technologies (freespace optics, liquid crystal on silicon, fiber couplers) appear critical, someone in terms of wavelength dependence, other one for insertion loss or device complexity [7]. In [8] MDM with modes that remain well spatially separated and with detection based on spatially separated photodetectors (PDs) is proposed for transmission over multimode fiber. Very recently, also optical vortices (OVs) carrying orbital angular momentum (OAM) [9]–[12] have been proposed instead of the LP modes to achieve MDM in free-space, demonstrating more feasible multiplexing and demultiplexing.

In this paper the inherent characteristics of fiber optical modes, in terms of shape and symmetry, are exploited to design an original MDM system with a MIMO receiver, which does not require optical demultiplexing, coherent detection, and DSP. In the paper the proposed MIMO is applied to two input modes in order to achieve double transmitted bit rate by means of direct detection and simple analog MIMO processing. We take two modes with propagation constants close to each other, leading to non-negligible intermodal crosstalk. In contrast, in [8] families of modes with well separated propagation constants and propagating in a fiber with very large core are adopted, leading to negligible intermodal crosstalk. The effectiveness of the proposed MDM solution is demonstrated using computer simulations both for two OVs and for two LP modes transmission, even in presence of large intermodal crosstalk. The proposed solution is a candidate for those high capacity MDM systems where cost, power consumption, and complexity, are relevant issues, such as local areas networks where thanks to the reduced reach chromatic and modal dispersion have not to be taken into account, also for high bit rate.

2. System model

Let us consider a MDM transmission in optical fiber based on the excitation of two modes, called mode 1 and mode 2, on-off keying modulated.

Both the excitation of OVs and of LP-modes can be considered for the proposed MDM system. In the following we consider only OV modes. The field distributions of fiber modes are given by the Laguerre-Gaussian fucntions. This assumption, which holds for parabolic index profile, can be used also to approximate other fiber index profiles, still maintaining the here exploited geometric and symmetry properties of the field. In particular, mode 1 is the fundamental mode OV_{01}, while mode 2 is OV_{11}. The OV_{01} and OV_{11} modes are characterized by the radial intensity profiles $R_1^2(\rho/\rho_0)$ and $R_2^2(\rho/\rho_0)$,respectively, that are

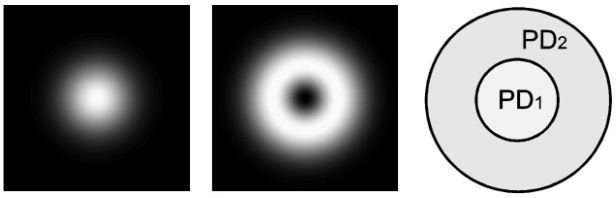

(a) (b) (c)

Figure 1: (a): intensity pattern of OV_{01}. (b): intensity pattern of OV_{11}. (c): inner circle PD_1 and outer circular annulus PD_2.

$$R_1^2(\rho/\rho_0) \propto e^{-\left(\frac{\rho}{\rho_0}\right)^2}, \qquad R_2^2(\rho/\rho_0) \propto \left(\frac{\rho}{\rho_0}\right)^2 e^{-\left(\frac{\rho}{\rho_0}\right)^2},$$

where ρ_0 is the characteristic size of the fundamental mode. Figure 1 shows the PDs structure matched to the choice of the input modes. The MIMO alphabet $\mathcal{A}$ is made by the four column vectors $\mathbf{a} = [a_1 \quad a_2]^T$, where the superscript ^{T} denotes vector or matrix transposition, and the bits a_1 and a_2 associated with modes 1 and 2, respectively, are assumed to be i.i.d. random variables taking their values with uniform probability in {0, 1}.
Owing to the fiber stress (twisting, bending, mechanical vibration) mode coupling during propagation can take place, leading to intermodal crosstalk. The fundamental mode generates the two sub-modes OV_{01}^{right} and OV_{01}^{left}, that are associated with electrical fields $\vec{E}_1(\rho,\theta)$ and $\vec{E}_2(\rho,\theta)$, both with radial intensity profile $R_1^2(\rho/\rho_0)$. Mode OV_{11} generates the four sub-modes OV_{11}^{+right}, OV_{11}^{-right}, OV_{11}^{+left}, and OV_{11}^{-left}, that are associated with the electrical fields $\vec{E}_3(\rho,\theta)$, $\vec{E}_4(\rho,\theta)$, $\vec{E}_5(\rho,\theta)$, and $\vec{E}_6(\rho,\theta)$, all with radial intensity profiles $R_2^2(\rho/\rho_0)$. The electrical field obtained from the intermodal crosstalk can be modelled as

$$\vec{E}(\rho,\theta.\mathbf{a}) = \vec{\mathbf{E}}(\rho,\theta)\cdot\mathbf{C}\cdot\mathbf{a},$$

where

$$\vec{\mathbf{E}}(\rho,\theta) = \left[\vec{E}_1(\rho,\theta) \quad \vec{E}_2(\rho,\theta) \quad \cdots \quad \vec{E}_6(\rho,\theta)\right] \tag{1}$$

and $\mathbf{C}$ is a 6×2 matrix consisting of the two columns corresponding to the two transmitted modes of the 6×6 unitary crosstalk matrix [13].

3. Mode separation by spatial demultiplexing

Separating the two modes after propagation using direct detection requires at least two spatially separated photodetectors. Direct detection by the 2 PDs gives the two signals

$$z_i(\mathbf{a}) = \int_{S_i} \left\|\vec{E}(\rho,\theta,\mathbf{a})\right\|^2 \rho\, d\rho\, d\theta, \qquad i=\{1,2\}, \tag{2}$$

where S_i is the surface of the i-th PD and $\|\cdot\|$ is the magnitude or L^2-norm operator. Thanks to the circular symmetry of PDs, the beating between any two fields is such that

$$\int_{S_i} \vec{E}_k(\rho,\theta)\cdot\vec{E}_h^*(\rho,\theta)\rho\, d\rho\, d\theta = \begin{cases} \int_{S_i} R_k^2(\rho/\rho_0)\,\rho\, d\rho\, d\theta, & k=h \\ 0 & k\neq h \end{cases},$$

Substituting (1) in (2) and using this orthogonality property, one gets the nonlinear MIMO model

$$\mathbf{z}(\mathbf{a}) = \mathbf{F}\cdot\mathbf{P}\cdot\mathbf{a} + \mathbf{w}(\mathbf{a}),$$

where $\mathbf{z}(\mathbf{a}) = [z_1(\mathbf{a}) \quad z_2(\mathbf{a})]^T$, $\mathbf{w}(\mathbf{a})$ is a 2×1 vector. The product $\mathbf{F}\cdot\mathbf{P}$ is

$$\begin{bmatrix} \int_{S_1} R_1^2(\rho/\rho_0)\,\rho\, d\rho\, d\theta & \int_{S_1} R_2^2(\rho/\rho_0)\,\rho\, d\rho\, d\theta \\ \int_{S_2} R_1^2(\rho/\rho_0)\,\rho\, d\rho\, d\theta & \int_{S_2} R_2^2(\rho/\rho_0)\,\rho\, d\rho\, d\theta \end{bmatrix} \cdot \begin{bmatrix} p_1 & 1-p_2 \\ 1-p_1 & p_2 \end{bmatrix},$$

where coefficients $0 \le p_1 \le 1$ and $0 \le p_2 \le 1$ that characterize the crosstalk are

$$p_1 = \|[c_{11} \quad c_{21}]\|^2 \qquad p_2 = \|[c_{32} \quad c_{42} \quad c_{52} \quad c_{62}]\|^2$$

and $\mathbf{C} = [c_{kh}]$**.** The term $\mathbf{w}(\mathbf{a})$ depends in a nonlinear manner on a:

$$\mathbf{w}(\mathbf{a}) = a_1 a_2 w\, \mathbf{i},$$

where $\mathbf{i} = [\sqrt{0.5} \quad -\sqrt{0.5}]^T$ and w is a random variable that depends on random matrix $\mathbf{C}$. Note that in [8], where intermodal crosstalk is negligible, one has that $\mathbf{P}$ is the identity matrix and that $\mathbf{w}(\mathbf{a})$ is zero.

4. MIMO detection

Considering short reach without optical amplifiers, the noisy signal after photodetection is $\mathbf{y} = \mathbf{z}(\mathbf{a}) + \mathbf{n}$, where $\mathbf{n}$ is an additive white Gaussian noise (AWGN) vector with variance σ_n^2 per PD. The optimal decision about the transmitted vector $\mathbf{a}$ is obtained from the maximum likelihood (ML) rule, which, when AWGN affects the received signal, is

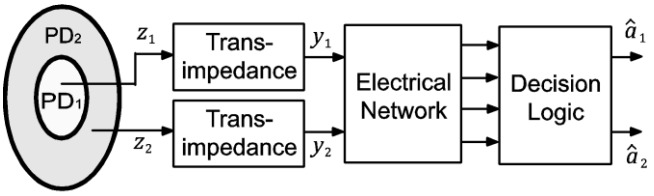

Figure 2: Receiver block diagram.

$$\hat{\mathbf{a}}_{\mathrm{ML}} = \arg\, min_{\mathbf{a}\in\mathcal{A}} \left(\mathbf{y} - \mathbf{z}(\mathbf{a})\right)^T \left(\mathbf{y} - \mathbf{z}(\mathbf{a})\right).$$

The block diagram of the receiver based on spatial demultiplexing is reported in Figure 2. The electrical network produces the four squared distances by biasing $\mathbf{y}$ by the four biases $\mathbf{z}(\mathbf{a})$ and then squaring the four results, and the decision logic, which can be based on few logic elements operating at symbol frequency, compares them and decides in favour of the vector $\mathbf{a}$ associated with the minimum squared distance.

5. Simulation results

Figure 3a reports the symbol error rate (SER) for $p_1 = p_1 = p$ against the ratio

$$R = \frac{E\{[z_2(\mathbf{a}) + z_2(\mathbf{a})]^2\}}{2\sigma_n^2},$$

where $E\{[z_2(\mathbf{a}) + z_2(\mathbf{a})]^2\}/2$ is proportional to the mean square of the optical power that reaches each PD. We adopt $E\{[z_2(\mathbf{a}) + z_2(\mathbf{a})]^2\}/2$ as a figure of merit because it depends on the input optical power only, while it is independent of the mode coupling affecting the fiber. In Figure 3b we show the optimization of the radius r of the inner circular PD, normalized to the characteristic size ρ_0, in order to maximize the distance d between $[0 \quad 1]^T$ and $[1 \quad 0]^T$ symbols. This radius is insensitive to p and R. Figure 3a shows that the sensitivity of the SER to p is moderate. Also, the figure shows that the ML rule for $p = 1$ is virtually optimal also for $p = 0.9$ and $p = 0.8$. The reason behind this can be seen from Figure 3c, where it is apparent that the error probability is dominated by errors between $[0 \quad 1]^T$ and $[1 \quad 0]^T$ and that the ML rule for $p = 1$ remains virtually optimal for discriminating between $[0 \quad 1]^T$ and $[1 \quad 0]^T$ also when crosstalk is present. As a consequence, detection can be based on a non-adaptive electrical network.

6. Conclusions

A nonlinear MIMO system exploiting the inherent characteristic of optical modes in fiber in a direct detection scheme based on circular concentric PDs has been proposed and compared to MIMO based on optical demultiplexing with direct detection. This nonlinear MIMO represents a general framework to handle different families of modes, both for OV and LP multiplexing. The advantage of this scheme is that the receiver does not require high-speed sampling and DSP to detect the transmitted bits, being devised here a low cost, low consumption solution, not requiring any adaptive network.

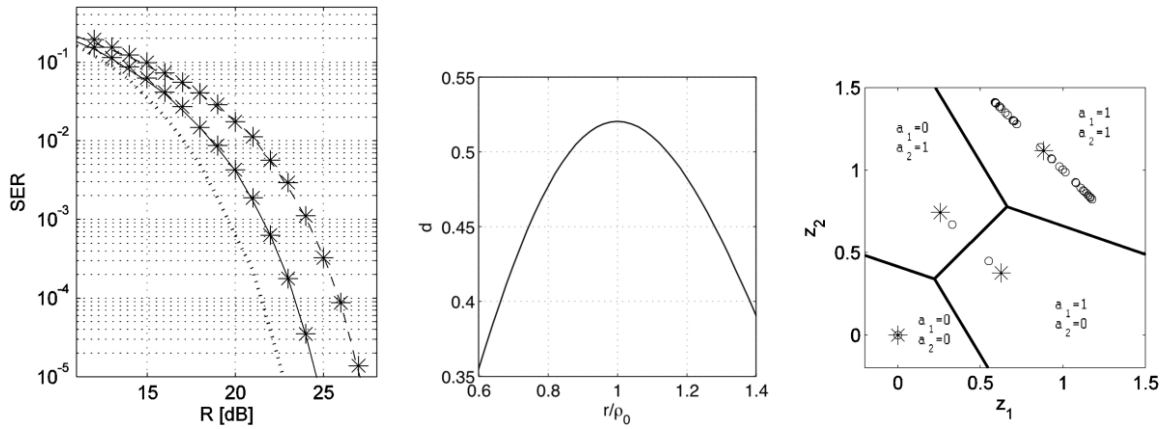

(a) (b) (c)

Figure 3: (a): SER versus R. Decision rule with $p = 1$ (dotted line); $p = 0.9$ (solid line); $p = 0.8$ (dashed line). Asterisks: suboptimal decision with ML rule for $p = 1$. (b): Distance d versus the ratio between the inner circular PD radius and ρ_0. (c): Decision regions: asterisks: $\mathbf{z}(\mathbf{a})$ with $p = 1$; circles: 20 realizations of $\mathbf{z}(\mathbf{a})$ with $p = 0.8$. The solid line bounds the decision regions of the ML rule for $p = 1$.

Bibliography

[1] G. Charlet et al., "WDM transmission at 6-Tbit/s capacity over transatlantic distance, using 42.7-Gb/s differential phase-shift keying without pulse carver," *J. Lightw. Technol.*, vol. 23, no. 1, pp. 104–107, Jan. 2005.

[2] P. Boffi et al., "Stable 100-Gb/s POLMUX-DQPSKtransmission with automatic polarization stabilization," *IEEE Photon. Technol. Lett.*, vol. 21, no. 11, pp. 745–747, 2009.

[3] V. Sleiffer et al., "Mode-division-multiplexed 3x112-Gb/s DP-QPSK transmission over 80 km few-mode fiber with inline MM-EDFA and Blind DSP," *Proc. ECOC 2012*, Tu.1.C.2, 2012.

[4] R. Ryf et al., "Mode-division multiplexing over 96 km of few-mode fiber using coherent 6×6 MIMO processing," J. Lightw. Technol., vol. 30, no. 4, pp. 521–531, Feb. 2012.

[5] M. Salsi et al., "Mode division multiplexed transmission with a weakly-coupled few-mode fiber," OFC 2012, OTu2C.5, 2012.

[6] C. Koebele et al., "40km transmission of five mode division multiplexed data streams at 100Gb/s with low MIMO-DSP complexity," Proc. ECOC 2011, Th.13.C.3, 2011.

[7] N. Hanzawa et al., "Mode-division multiplexed transmission with fiber mode couplers," Proc. OFC 2012, OW1D.4, 2012.

[8] C. P. Tsekrekos et al., "Design Considerations for a Transparent Mode Group Diversity Multiplexing Link," in Phot. Technol. Lett., vol. 18, no. 22, pp. 2359–2361, Nov. 2006.

[9] P. Martelli et al., "Free-space optical transmission with orbital angular momentum division multiplexing," Electron. Lett., vol. 47, no. 17, pp. 972–973, Aug. 2011.

[10] A. Gatto et al., "Free-space orbital angular momentum division multiplexing with Bessel beams," J. Optics, vol. 13, no. 6, Apr. 2011.

[11] J. Wang et al., "Terabit free-space data transmission employing orbital angular momentum multiplexing," Nat. Photonics, vol. 6, pp. 488–496, Jun. 2012.

[12] N. Bozinovic et al., "Orbital Angular Momentum (OAM) Based Mode Division Multiplexing (MDM) over a Km-length Fiber," Proc. ECOC 2012, Th.3.C.6, 2012.

[13] R. Dar et al., "The underaddressed optical multiple-input, multiple-output channel: capacity and outage," Opt. Lett., vol. 37, no. 15, pp. 3150–3152, July 2012.